Phase transition and thermal expansion property of $Cr_{2-x}Zr_{0.5x}Mg_{0.5x}Mo_3O_{12}$ solid solution*

Song Wen-Bo(宋文博)[a], Wang Jun-Qiao(王俊俏)[a], Li Zhi-Yuan(李志远)[a], Liu Xian-Sheng(刘献省)[a], Yuan Bao-He(袁保合)[a,b], and Liang Er-Jun(梁二军)[a]†

[a] School of Physical Science & Engineering and Key Laboratory of Materials Physics of Ministry of Education of China, Zhengzhou University, Zhengzhou 450052, China

[b] North China University of Water Resources and Electric Power, Zhengzhou 450011, China

(Received 10 October 2013; revised manuscript received 27 December 2013; published online 10 April 2014)

Compounds with the formula $Cr_{2-x}Zr_{0.5x}Mg_{0.5x}Mo_3O_{12}$ ($x = 0.0$, 0.3, 0.5, 0.9, 1.3, 1.5, 1.7, 1.9) are synthesized, and the effects of Zr^{4+} and Mg^{2+} co-incorporation on the phase transition, thermal expansion, and Raman mode are investigated. It is found that $Cr_{2-x}Zr_{0.5x}Mg_{0.5x}Mo_3O_{12}$ crystallize into monoclinic structures for $x \leq 1.3$ and orthorhombic structures for $x \geq 1.5$ at room temperature. The phase transition temperature from a monoclinic to an orthorhombic structure of $Cr_2Mo_3O_{12}$ can be reduced by the partial substitution of $(ZrMg)^{6+}$ for Cr^{3+}. The overall linear thermal expansion coefficient decreases with the increase of the $(ZrMg)^{6+}$ content in an orthorhombic structure sample. The co-incorporation of Zr^{4+} and Mg^{2+} in the lattice results in the occurrence of new Raman modes and the hardening of the symmetric vibrational modes, which are attributed to the MoO_4 tetrahedra sharing corners with ZrO_6/MgO_6 octahedra and to the strengthening of Mo–O bonds due to less electronegativities of Zr^{4+} and Mg^{2+} than Cr^{3+}, respectively.

Keywords: negative thermal expansion material, phase transition, Raman spectroscopy

PACS: 65.40.De, 61.50.Ks, 78.30.–j **DOI:** 10.1088/1674-1056/23/6/066501

1. Introduction

The majority of known materials have positive coefficients of thermal expansion (CTE), i.e., they expand on heating and contract on cooling. The rediscovery of negative thermal expansion (NTE) in cubic ZrW_2O_8[1–3] (AM_2O_8 family) in a large temperature range sheds light on the possibility of tailoring the CTEs in pure and composite materials. Besides the AM_2O_8 family, several other open-framework families, such as AO_3,[4] AMO_5,[5] AM_2O_7,[6] A_2O,[7] and $A_2M_3O_{12}$[8–12] have been found to exhibit low thermal expansion or NTE. Recently, the compounds with the general chemical formula ABM_3O_{12} ($A = Hf^{4+}$ or Zr^{4+}; $B = Mg^{2+}$; $M = W^{6+}$ or Mo^{6+})[13–17] with another orthorhombic structure have been reported to exhibit low or negative thermal expansion.

Materials with general formula $A_2M_3O_{12}$, where 'A' is a trivalent cation (Al, Y, Fe or a lanthanum group element) and M is W or Mo, crystallize into either orthorhombic or monoclinic symmetric structures, depending on the A^{3+} cation size.[3] The members of the $A_2M_3O_{12}$ family with larger A^{3+} cations crystallize into orthorhombic structures (space group $pbcn$) and exhibit negative overall linear thermal expansion coefficients while the ones with smaller A^{3+} cations crystallize into monoclinic structures (space group $P2_1/a$) and display positive thermal expansions.[18,19] The orthorhombic ones each have an open framework structure with A–O–M linkages, which can accommodate the transverse thermal vibrations responsible for NTE, while the monoclinic ones have an edge-shared structure, which is more densely packed and cannot accommodate the transverse thermal vibrations. In other words, that the materials of the $A_2M_3O_{12}$ family with smaller A^{3+} cation size give rise to NTE is possible only after monoclinic-to-orthorhombic phase transition at higher temperatures. For example, $Al_2Mo_3O_{12}$, $Cr_2Mo_3O_{12}$, and $Fe_2Mo_3O_{12}$ crystallize into monoclinic structures at room temperature and transform from monoclinic to orthorhombic around 473 K, 676 K, and 785 K, respectively, and their CTEs in the orthorhombic structure are 2.389×10^{-6} K^{-1}, 0.67×10^{-6} K^{-1}, and 1.72×10^{-6} K^{-1} indicated by X-ray diffraction (XRD)[19] and -2.83×10^{-6} K^{-1}, -9.39×10^{-6} K^{-1}, and -14.82×10^{-6} K^{-1} obtained by dilatometry.[20] There are large misfits between the linear CTEs measured by diffraction and dilatometric methods for this family of materials. There are probably several extrinsic sources causing the discrepancy, but by far the most cited one is the formation of microcracks on cooling due to the anisotropic thermal expansion of these phases.[21] We believe that the large difference in CTE between monoclinic (large positive CTEs) and orthorhombic (low or negative CTEs) structures and the anisotropic nature of the materials are the main reasons for the microcracks dur-

*Project supported by the National Natural Science Foundation of China (Grant Nos. 10974183 and 11104252), the Science Fund of the Ministry of Education of China (Grant No. 20114101110003), the Fund for Science & Technology Innovation Team of Zhengzhou City, China (Grant No. 112PCXTD337), and the Postdoctoral Research Sponsorship in Henan Province, China (Grant No. 2011002).

†Corresponding author. E-mail: ejliang@zzu.edu.cn

© 2014 Chinese Physical Society and IOP Publishing Ltd

ing temperature change, and are responsible for the discrepancy in CTEs measured by different methods. To reduce the monoclinic-to-orthorhombic phase-transition temperature to below room temperature for this family of materials with smaller A^{3+} cation size is essential for applications and still remains a challenge.

Recently, Ari M, Jardim P M, Marinkovic, *et al.*[19] synthesized $Cr_{2x}Fe_{2-2x}Mo_3O_{12}$, $Al_{2x}Cr_{2-2x}Mo_3O_{12}$, and $Al_{2x}Fe_{2-2x}Mo_3O_{12}$ to study the effect of the cation substitution on the phase transition temperature from monoclinic to orthorhombic structure in the $A_2M_3O_{12}$ family. They found a linear relationship between the transition temperature and the fraction of A^{3+} cations (x) for each system and confirmed that the phase transition temperature decreases with the increase of electronegativity of A^{3+} cations.

It was found recently that the A^{3+} cation can not only be a transition metal or rare earth that occupies an octahedral position, but also be substituted by a mixture of tetravalent and bivalent cations, such as $HfMgW_3O_{12}$,[13,14] $HfMgMo_3O_{12}$,[15] $ZrMgMo_3O_{12}$.[17] These materials exhibit low or negative linear thermal expansion ($\alpha_l = -0.77 \times 10^{-6}$ K^{-1},[13] $\alpha_l = -1.2 \times 10^{-6}$ K^{-1}[14] for $HfMgW_3O_{12}$, $\alpha_l = 1.02 \times 10^{-6}$ K^{-1} for $HfMgMo_3O_{12}$,[15] $\alpha_l = -3.73 \times 10^{-6}$ K^{-1} for $ZrMgMo_3O_{12}$[17]). Kimberly *et al.*[22] reported on $In(HfMg)_{0.5}Mo_3O_{12}$, which exhibited a phase transition from monoclinic ($P2_1/a$) to orthorhombic ($Pnma$) structure at about 425 K, and NTE ($\alpha_l = -0.4 \times 10^{-6}$ K^{-1}) from 500 K–900 K. Suzuki and Omote[23] synthesized $Al_{2x}(HfMg)_{1-x}W_3O_{12}$ which shows a low CTE ($\alpha_l = 2 \times 10^{-6}$ K^{-1}–2×10^{-6} K^{-1} for $x = 0$–0.7). A near zero thermal expansion was found for $x = 0.15$.

In this paper, we synthesize the materials with the formula $Cr_{2-x}Zr_{0.5x}Mg_{0.5x}Mo_3O_{12}$ ($x = 0.0$, 0.3, 0.5, 0.9, 1.3, 1.5, 1.7, 1.9). The crystal structures and thermal expansion properties for this family of materials are investigated by room-temperature and high temperature X-ray diffractions and dilatometer. The phase transitions are studied by Raman spectroscopy and differential scanning calorimetry.

2. Experiment

$Cr_{2-x}Zr_{0.5x}Mg_{0.5x}Mo_3O_{12}$ ($x = 0$, 0.3, 0.5, 0.9, 1.3, 1.5, 1.7, and 1.9) were produced by solid-state reaction from a stoichiometric mixture of Cr_2O_3, ZrO_2, MgO, and MoO_3 (99.9% purity). The mixtures were ground in a mortar for 2 h, sintered in a tubular furnace at 1173 K for 8 h and then cooled down slowly.

X-ray diffraction (XRD) of the samples was carried out with an X' Pert PRO X-ray diffractometer. The microstructures were studied using a JSM-6700F scanning electron microscope (SEM). A Renishaw MR-2000 Raman spectrometer with 532-nm wavelength laser excitation was used for Raman spectroscopic studies. The temperature dependence of the Raman spectra was recorded using a TMS 94 heating/freezing stage from Linkam Scientific Instruments Ltd, within an accuracy of ±0.1 K. The differential scanning calorimetry (DSC) studies were carried out on an Ulvac Sinku-Riko DSC, Model 1500M/L with the heating and cooling rates of 10 K/min. The linear thermal expansion coefficients were measured by a dilatometer (LINSEIS L75).

The unit-cell and crystal structure parameters are refined from X-ray diffraction patterns through the Rietveld methods, using the program Fullprof. The crystal structures of monoclinic $Fe_2Mo_3O_{12}$ (ICSD 16402) and orthorhombic $Fe_2Mo_3O_{12}$ (ICSD 80449) were used as the starting model for $Cr_{2-x}Zr_{0.5x}Mg_{0.5x}Mo_3O_{12}$.

3. Results and discussion

3.1. Crystal structure and phase transition

Phase identifications of the samples with different values of $(ZrMg)^{6+}$ content are performed by means of X-ray diffraction at room temperature (RT). Figure 1 shows the RT XRD patterns of $Cr_{2-x}Zr_{0.5x}Mg_{0.5x}Mo_3O_{12}$ ($x = 0$, 0.3, 0.5, 0.9, 1.3, 1.5, 1.7, and 1.9). The RT unit cell parameters of $Cr_{2-x}Zr_{0.5x}Mg_{0.5x}Mo_3O_{12}$ are tabulated in Table 1.

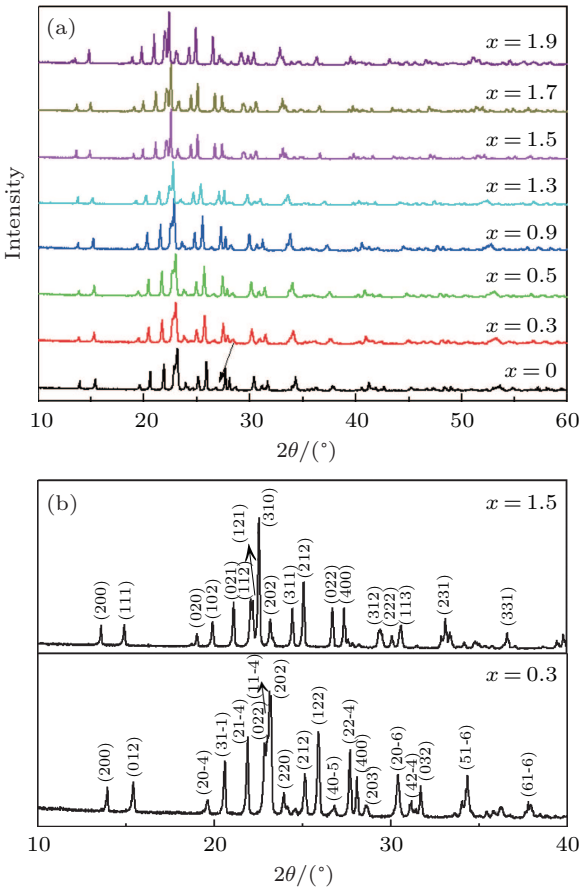


Fig. 1. (a) X-ray diffraction patterns of $Cr_{2-x}Zr_{0.5x}Mg_{0.5x}Mo_3O_{12}$ for various values of x, and (b) the partially enlarged X-ray diffraction patterns of $Cr_{2-x}Zr_{0.5x}Mg_{0.5x}Mo_3O_{12}$ for $x = 0.3$ and $x = 1.5$ at room temperature.

Table 1. Unit cell parameters of $Cr_{2-x}Zr_{0.5x}Mg_{0.5x}Mo_3O_{12}$ at room temperature.

x	a/Å	b/Å	c/Å	β/(°)
0	15.5584(5)	9.1563(2)	18.0982(6)	125.3018(22)
0.1	15.5885(10)	9.1756(5)	18.1423(12)	125.3371(41)
0.3	15.6456(9)	9.2112(4)	18.2096(10)	125.3454(37)
0.5	15.7110(8)	9.2516(4)	18.2892(9)	125.3649(33)
0.7	15.7602(10)	9.2809(4)	18.3477(11)	125.3792(41)
0.9	15.8043(8)	9.3079(3)	18.3962(8)	125.3907(3)
1.1	15.8612(6)	9.3421(3)	18.4655(6)	125.4205(28)
1.3	15.9262(15)	9.3836(5)	18.5483(13)	125.4819(66)
1.5	13.0209(6)	9.3818(4)	9.4773(4)	
1.7	13.0825(7)	9.4271(5)	9.5205(5)	

It is known that $Cr_2Mo_3O_{12}$ crystallizes into a monoclinic $Fe_2Mo_3O_{12}$-type structure (ICDD-PDF No.00-031-0642). The XRD patterns of the molybdates for $x = 0.0$–1.3 remain unchanged except successive shifts of the diffraction peaks toward smaller angles with the increase of $(ZrMg)^{6+}$ content, suggesting that they keep the monoclinic structure until $x = 1.3$. The shifts of the peaks indicate a progressive increase in lattice constant due to the average cation radius of $(ZrMg)^{6+}$ (72 pm) being bigger than that of Cr^{3+} (61.5 pm). While for $x = 1.5$ and 1.7 the molybdates exhibit an orthorhombic $Fe_2Mo_3O_{12}$-type structure (ICDD-PDF No.00-033-0661) as indicated by the disappearance of the XRD peak at 26.69°, which is characteristic of the phase transition from a monoclinic to an orthorhombic structure. However, by comparison with the previously reported XRD patterns for $HfMgW_3O_{12}$[13,14] and $HfMgMo_3O_{12}$,[15] it can be concluded that the molybdate for $x = 1.9$ has the orthorhombic symmetry with space group *Pnma* (62) or $Pna2_1$ (33) at room temperature.

In Fig. 2, we show the typical scanning electron microscopy (SEM) images of the cross section for the $Cr_{0.5}Zr_{0.75}Mg_{0.75}Mo_3O_{12}$ and $Cr_{0.3}Zr_{0.85}Mg_{0.85}Mo_3O_{12}$ ceramic blocks. The samples exhibit microstructures with closely packed polygonals and the grain sizes range from 2 μm to 8 μm. The average grain size for $Cr_{0.5}Zr_{0.75}Mg_{0.75}Mo_3O_{12}$ is smaller than that of $Cr_{0.3}Zr_{0.85}Mg_{0.85}Mo_3O_{12}$.

Figure 3 shows the temperature-dependent Raman spectra (TDRS) for $Cr_2Mo_3O_{12}$. By comparison with the Raman spectra of other molybdates, such as $Y_2Mo_3O_{12}$[18] and $Fe_2Mo_3O_{12}$,[19,20,24] the Raman modes from 900 cm^{-1} to 1050 cm^{-1}, from 750 cm^{-1} to 900 cm^{-1}, and from 300 cm^{-1} to 400 cm^{-1} can be identified as the internal symmetric stretching, asymmetric stretching, and bending vibrations of the MoO_4 tetrahedra, whereas those below 300 cm^{-1} are translational and librational motions of the polyhedra. The Raman band at 994 cm^{-1} becomes weak gradually with the increase of temperature and vanishes when the temperature is increased to 653 K. This is an indication that the monoclinic-to-orthorhombic phase transition of $Cr_2Mo_3O_{12}$ occurs between 648 K and 653 K, in accordance with its phase transition temperature reported by Tyagi *et al.*[20] and by Ari *et al.*[19] Therefore, the Raman spectra above 653 K are characteristic of the orthorhombic $Cr_2Mo_3O_{12}$.

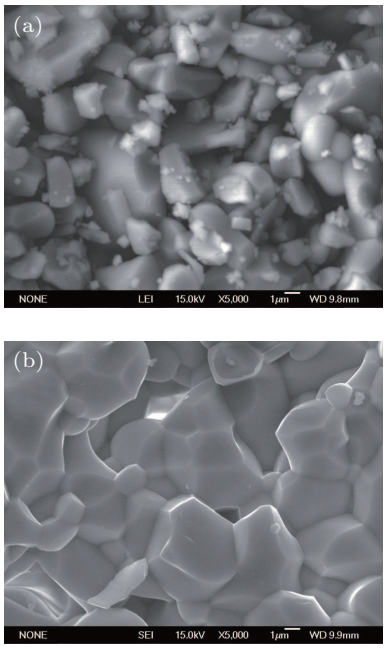


Fig. 2. (color online) SEM micrographs of (a) $Cr_{0.5}Zr_{0.75}Mg_{0.75}Mo_3O_{12}$ and (b) $Cr_{0.3}Zr_{0.85}Mg_{0.85}Mo_3O_{12}$.

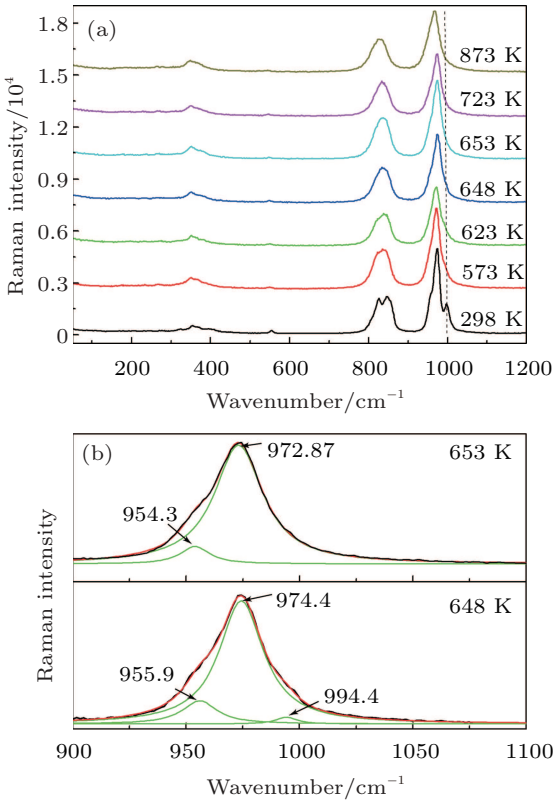


Fig. 3. (color online) (a) Raman spectra of $Cr_2Mo_3O_{12}$ at different temperatures and (b) enlarged portion of the symmetric stretching modes fitted with Lorentz line profiles.

Figure 4 shows the temperature dependences of the Raman spectra of $Cr_{1.5}Zr_{0.25}Mg_{0.25}Mo_3O_{12}$. It is shown that $Cr_{1.5}Zr_{0.25}Mg_{0.25}Mo_3O_{12}$ crystallized into a monoclinic structure at room temperature, as evidenced by the appearance of the Raman band at about 998 cm^{-1}. With the increase of temperature, this Raman band becomes weak gradually and vanishes when the temperature increases to 523 K (see Fig. 4(b)), suggesting that the monoclinic-to-orthorhombic phase transition of $Cr_{1.5}Zr_{0.25}Mg_{0.25}Mo_3O_{12}$ occurs at about 523 K, about 150 K lower than that of $Cr_2Mo_3O_{12}$. The reduction in phase transition temperature by $(ZrMg)^{6+}$ substitution not only confirms the formation of solid solution $Cr_{1.5}Zr_{0.25}Mg_{0.25}Mo_3O_{12}$ but also gives us hope to further lower the phase transition temperature to below room temperature by increasing the substitution of $(ZrMg)^{6+}$ for Cr^{3+}. This is important for applications of the materials.

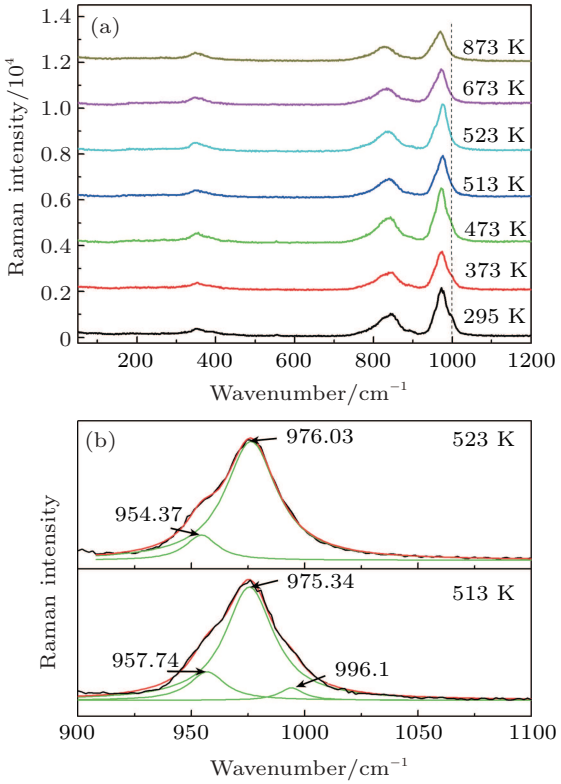


Fig. 4. (color online) (a) Raman spectra of $Cr_{1.5}Zr_{0.25}Mg_{0.25}Mo_3O_{12}$ at different temperatures and (b) enlarged portion of the symmetric stretching modes fitted with Lorentz line profiles.

The temperature-dependent Raman spectra of the samples with further increasing the $(ZrMg)^{6+}$ content are measured. It is shown that the phase transition temperature of $Cr_{2-x}Zr_{0.5x}Mg_{0.5x}Mo_3O_{12}$ can be further lowered with the increase of $(ZrMg)^{6+}$ content so that it is well below room temperature when $x > 1.4$. Figure 5 shows the temperature-dependent Raman spectra of $Cr_{0.3}Zr_{0.85}Mg_{0.85}Mo_3O_{12}$. From the comparison of room-temperature Raman spectrum between $Cr_2Mo_3O_{12}$ and $Cr_{0.3}Zr_{0.85}Mg_{0.85}Mo_3O_{12}$, it can be concluded that $Cr_{0.3}Zr_{0.85}Mg_{0.85}Mo_3O_{12}$ crystallized already into an orthorhombic structure at room temperature since the Raman band at about 996 cm^{-1}, characteristic of the monoclinic phase, does not appear for this composition. To determine the operating temperature range of the orthorhombic phase, we pursue the study of its orthorhombic-to-monoclinic phase transition by reducing temperature. However, no phase transition is found from 298 K to 103 K. It can be deduced that the material of $Cr_{0.3}Zr_{0.85}Mg_{0.85}Mo_3O_{12}$ keeps the orthorhombic structure until a very low temperature ($T <$ 103 K).

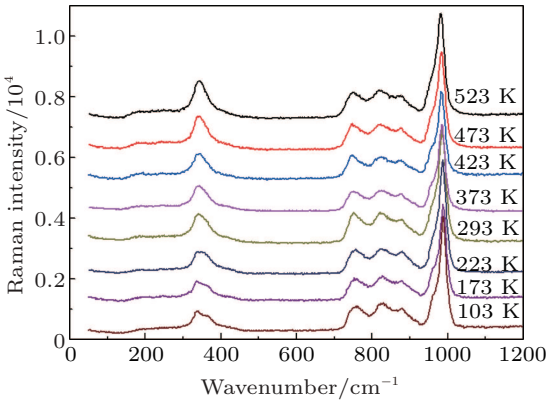


Fig. 5. (color online) Raman spectra of $Cr_{0.3}Zr_{0.85}Mg_{0.85}Mo_3O_{12}$ at different temperatures.

The effective decrease of the phase transition temperature by increasing the substitution of $(ZrMg)^{6+}$ for Cr^{3+} revealed by Raman spectroscopy is confirmed by DSC. Figure 6 shows the DSC curves of $Cr_{2-x}Zr_{0.5x}Mg_{0.5x}Mo_3O_{12}$ for $x = 0.0$, 0.3, 0.7, 1.1. It shows clearly that the monoclinic-to-orthorhombic phase transition temperature decreases with the increase of the amount of $(ZrMg)^{6+}$ as indicated by the endothermic peak on each curve.

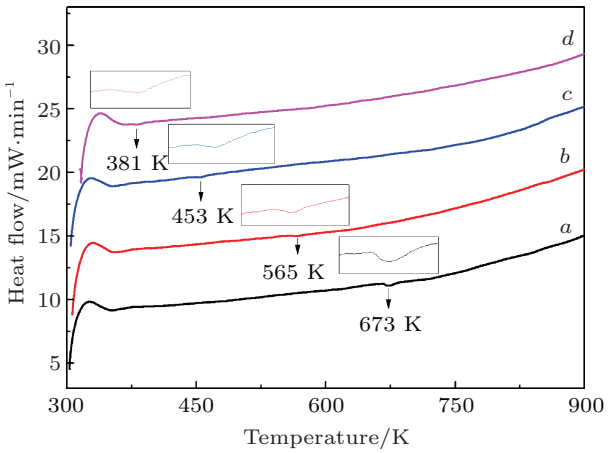


Fig. 6. (color online) Typical differential scanning calorimetry curves for $Cr_{2-x}Zr_{0.5x}Mg_{0.5x}Mo_3O_{12}$ at $x = 0$ (curve *a*), 0.3 (curve *b*), 0.7 (curve *c*), and 1.1 (curve *d*). The insets show the enlarged views of the endothermic peaks.

3.2. Thermal expansion properties

As mentioned above, the materials of the $A_2M_3O_{12}$ family with smaller A^{3+} cation sizes give rise to a low thermal

expansion or NTE after the transition from monoclinic to orthorhombic phase at higher temperatures. The XRD patterns of $Cr_{0.5}Zr_{0.75}Mg_{0.75}Mo_3O_{12}$ and $Cr_{0.3}Zr_{0.85}Mg_{0.85}Mo_3O_{12}$ in a temperature range of 300 K–1000 K are measured and their structure refinements are carried out by the Rietveld method using the program Fullprof. Figure 7 shows the result of the Rietveld analysis of the XRD patterns of $Cr_{0.5}Zr_{0.75}Mg_{0.75}Mo_3O_{12}$ at 500 K. The cell parameters for $x = 1.5$ and 1.7 at different temperatures are calculated by using the method of Rietveld refinement and are shown in Fig. 8. The average axial CTEs from 400 K to 1000 K are calculated to be $\alpha_a = 6.19 \times 10^{-6}$ K^{-1}, $\alpha_b = -6.2 \times 10^{-7}$ K^{-1}, and $\alpha_c = -2.44 \times 10^{-6}$ K^{-1} for $Cr_{0.5}Zr_{0.75}Mg_{0.75}Mo_3O_{12}$ and $\alpha_a = 5.82 \times 10^{-6}$ K^{-1}, $\alpha_b = -1.27 \times 10^{-6}$ K^{-1}, and $\alpha_c = -2.68 \times 10^{-6}$ K^{-1} for $Cr_{0.3}Zr_{0.85}Mg_{0.85}Mo_3O_{12}$. This gives rise to a linear CTEs ($\alpha_l = \alpha_V/3$,) of $\alpha_l = 1.04 \times 10^{-6}$ K^{-1} and $\alpha_l = 0.62 \times 10^{-6}$ K^{-1} for $x = 1.5$ and $x = 1.7$, respectively. It is evident that the anisotropy of the materials decreases with the amount of $(ZrMg)^{6+}$ increasing.

It can be seen that the a axes of both samples expand with the increase of temperature while the b axis and c axis expand from RT to 400 K and then contract. The more abnormal expansions of the b and c axes than the a axis from RT to 400 K should not be attributed to phase transition of the materials since they are already in orthorhombic phase at room temperature as analyzed above. We attribute it to the release of water species in the microchannels of the building block structure with the increase of temperature. The water species can make the b axis and c axis contract much more than the a axis and hence the release of the water species leads to a more abrupt expansion of the b and c axes than the a axis, as revealed in our previous papers.[10,24] However, the quantity of the water species is small since it is not detected by Raman spectroscopy and DSC. In order to confirm the influence of the water species on the thermal expansion property, we measure the length change of a ceramic rod for the composition of $Cr_{0.3}Zr_{0.85}Mg_{0.85}Mo_3O_{12}$ 10 min, 2 h, 12 h, and 48 h after having been heated at 473 K, respectively (see Fig. 9). It shows that the coefficient of thermal expansion in the low temperature range increases with time, while that above the release

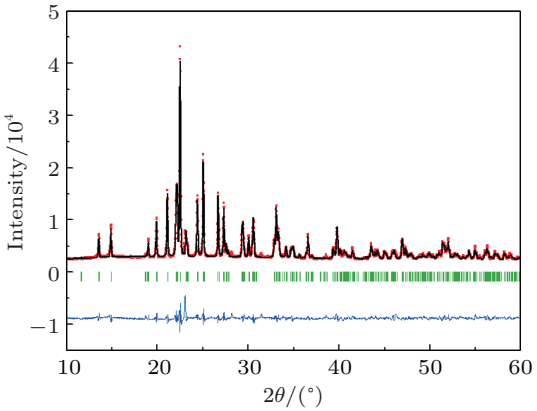


Fig. 7. (color online) Result of the Rietveld analysis of the XRD pattern of $Cr_{0.5}Zr_{0.75}Mg_{0.75}Mo_3O_{12}$ at 500 K ($R_p = 13.5\%$, $R_{wp} = 14.7\%$, and $R_{exp} = 3.85\%$). The "+" signs represent the observed profiles. The solid line represents the calculated profile. Vertical bars indicate the positions of Bragg peaks for this phase. The lowest curve refers to the difference between the observed and calculated patterns.

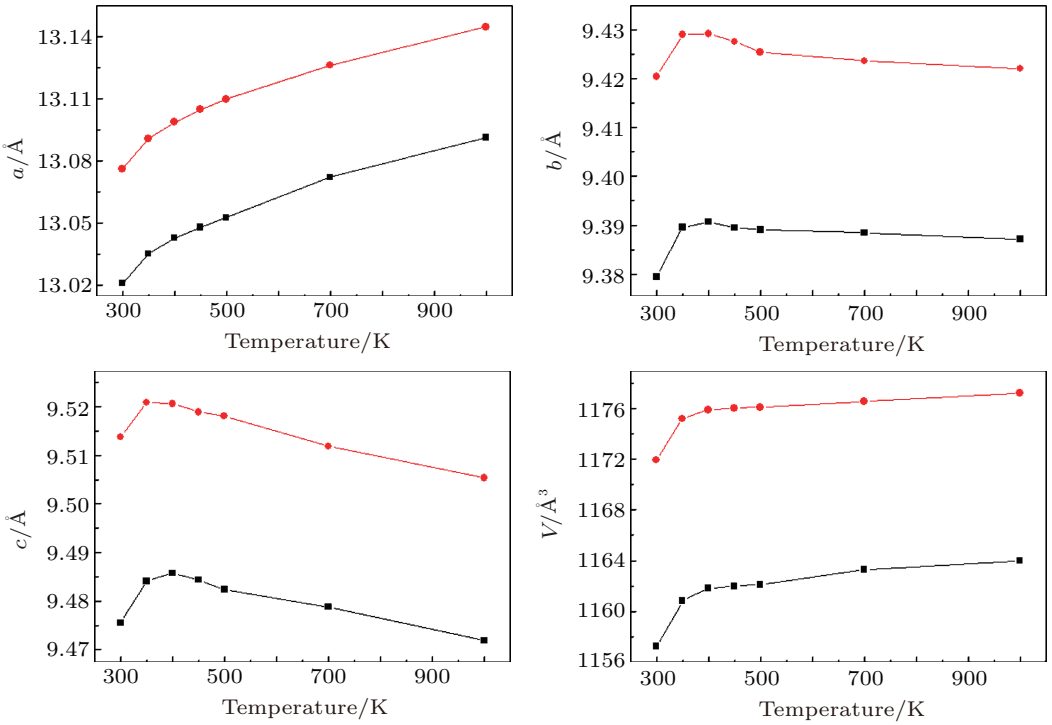


Fig. 8. (color online) Lattice parameters of $Cr_{0.5}Zr_{0.75}Mg_{0.75}Mo_3O_{12}$ (■ symbols) and $Cr_{0.3}Zr_{0.85}Mg_{0.85}Mo_3O_{12}$ (● symbols) at different temperatures.

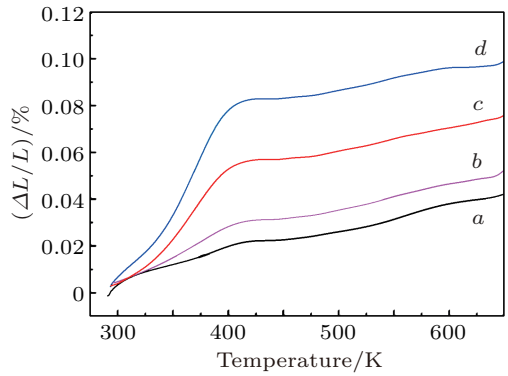


Fig. 9. (color online) Length changes of the ceramic rod of $Cr_{0.3}Zr_{0.85}Mg_{0.85}Mo_3O_{12}$ measured (curve *a*) 10 min, (curve *b*) 2 h, (curve *c*) 12 h, and (curve *d*) 48 h after having been heated at 473 K.

temperature of crystal water remains unchanged, confirming our analyses above. When the materials have been kept in air for a longer time, more water molecules would be admitted.

The linear CTEs of $Cr_{2-x}Zr_{0.5x}Mg_{0.5x}Mo_3O_{12}$ ($x = 1.5$, 1.7, and 1.9) measured with a dilatometer are 1.4×10^{-6} K^{-1}, 1.2×10^{-6} K^{-1}, and 0.75×10^{-6} K^{-1} from 393 K–673 K for $Cr_{0.5}Zr_{0.75}Mg_{0.75}Mo_3O_{12}$, $Cr_{0.3}Zr_{0.85}Mg_{0.85}Mo_3O_{12}$, and $Cr_{0.1}Zr_{0.95}Mg_{0.95}Mo_3O_{12}$, respectively. The CTEs of $Cr_{2-x}Zr_{0.5x}Mg_{0.5x}Mo_3O_{12}$ ($x = 1.5$, 1.7, and 1.9) obtained by dilatometer decrease with the increase of $(ZrMg)^{6+}$ content for the orthorhombic materials, which is similar to the Rietveld analysis results. It is noticed that the CTEs measured by XRD and dilatometer by us are very close, which we attribute to the low thermal expansion property of the orthorhombic phase in the large temperature range and lower anisotropy after co-incorporation of Zr^{4+} and Mg^{2+}.

In order to see the effect of $(ZrMg)^{6+}$ incorporation on the vibrational modes, we compare in Fig. 10 the Raman spectra of $Cr_{2-x}Zr_{0.5x}Mg_{0.5x}Mo_3O_{12}$ for $x = 0$, 0.5, 0.9, 1.1, 1.3, 1.5, 1.7, and 1.9. It is obvious that there are more Raman modes with the increase of $(ZrMg)^{6+}$ content, though the characteristic Raman mode at about 998 cm^{-1} vanishes. As discussed above, the disappearance of this band is an indication of the orthorhombic phase formation ($x \geq 1.5$). Co-incorporation of $(ZrMg)^{6+}$ replaces part of Cr^{3+} in the lattice, making the MoO_4 tetrahedra share corners with ZrO_6 and MgO_6 octahedra besides with CrO_6. We attribute, therefore, the additional Raman bands in the asymmetric stretching region with incorporation of $(ZrMg)^{6+}$ to the Mo–O asymmetric stretching vibrations originating from the MoO_4 tetrahedra sharing corners with ZrO_6 and MgO_6 octahedra.

It is also noticed that the asymmetric stretching Raman bands in orthorhombic $Cr_2Mo_3O_{12}$ shift obviously toward higher wavenumbers after incorporation of $(ZrMg)^{6+}$ (Fig. 11), indicating the hardening of the bands. Cr^{3+} has an electronegativity of 1.66 which is larger than Zr^{4+} (1.33) and Mg^{2+} (1.31). This means that Zr^{4+} and Mg^{2+} ions have a lower ability than Cr^{3+} ions to attract electrons from the bridging "O" ions and hence the incorporation of $(ZrMg)^{6+}$ leads to the strengthening of the Mo–O bonds. The Mo–O bonds become stronger with the increase of $(ZrMg)^{6+}$ content and therefore a blue shift of the stretching Raman band occurs.

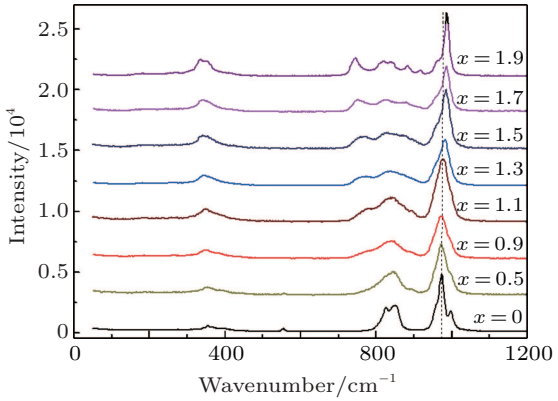


Fig. 10. (color online) Raman spectra of $Cr_{2-x}Zr_{0.5x}Mg_{0.5x}Mo_3O_{12}$ ($x = 0$, 0.5, 0.9, 1.1, 1.3, 1.5, 1.7, and 1.9) at room temperature.

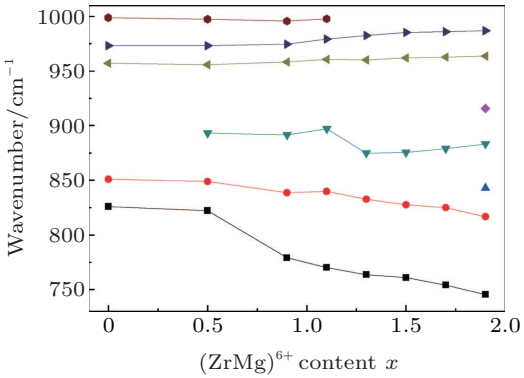


Fig. 11. (color online) Dependences of the stretching mode position on substitution amount of $(ZrMg)^{6+}$. The Raman band positions are derived from curve fittings of Lorentz line profile.

4. Conclusions

The solid solutions with the formula $Cr_{2-x}Zr_{0.5x}Mg_{0.5x}Mo_3O_{12}$ ($x = 0.0$–1.9) are synthesized, and the effects of Zr^{4+} and Mg^{2+} co-incorporation on the phase transition, thermal expansion, and Raman mode changes are investigated by XRD, Raman spectroscopy, and DSC. It is shown that $Cr_{2-x}Zr_{0.5x}Mg_{0.5x}Mo_3O_{12}$ crystallize into monoclinic structures for $x \leq 1.3$ and into orthorhombic structures for $x \geq 1.5$. The phase transition temperature from monoclinic to orthorhombic structure can be effectively reduced with the increase of $(ZrMg)^{6+}$ content so that the $Cr_{2-x}Zr_{0.5x}Mg_{0.5x}Mo_3O_{12}$ for $x \geq 1.5$ crystallize into orthorhombic phase at room temperature and keep this structure until a very low temperature. The overall linear thermal expansion coefficients decrease with the increase of $(ZrMg)^{6+}$ content for the orthorhombic materials. The calculated linear thermal expansion coefficients from 400 K–1000 K are $1.04 \times$

10^{-6} K^{-1} and 0.62×10^{-6} K^{-1} for $x = 1.5$ and $x = 1.7$, respectively. The co-incorporation of Zr^{4+} and Mg^{2+} into the lattice results in the occurrence of more Raman modes and the hardening of the symmetric stretching modes, which are attributed to the MoO_4 tetrahedra sharing corners with ZrO_6/MgO_6 octahedra and to the strengthening of Mo–O bonds due to less electronegativities of Zr^{4+} and Mg^{2+} than Cr^{3+}, respectively.

References

[1] Mary T A, Evans J S O, Vogt T and Sleight A W 1996 *Science* **272** 90
[2] Perottoni C A and Da Jornada J A H 1998 *Science* **280** 886
[3] Liang E J 2010 *Recent Pat. Mater. Sci.* **3** 106
[4] Chatterji T, Hansen T C, Brunelli M and Henry P F 2009 *Appl. Phys. Lett.* **94** 241902
[5] Amos T G, Yokochi A and Sleight A W 1998 *J. Solid State Chem.* **141** 303
[6] Yuan H L, Yuan B H, Li F and Liang E J 2012 *Acta Phys. Sin.* **61** 226502 (in Chinese)
[7] Kennedy B J, Kubota Y and Kato K 2005 *Solid State Commun.* **136** 177
[8] Evans J S O, Mary T A and Sleight A W 1998 *J. Solid State Chem.* **137** 148
[9] Liang E J, Huo H L, Wang Z, Chao M J and Wang J P 2009 *Solid State Sci.* **11** 139
[10] Li Q J, Yuan B H, Song W B, Liang E J and Yuan B 2012 *Chin. Phys. B* **21** 046501
[11] Wu M M, Peng J, Zu Y, Liu R D, Hu Z B, Liu Y T and Chen D F 2012 *Chin. Phys. B* **21** 116102
[12] Liu F S, Chen X P, Xie H X, Ao W Q and Li J Q 2010 *Acta Phys. Sin.* **59** 3350 (in Chinese)
[13] Suzuki T and Omote A 2004 *J. Am. Ceram. Soc.* **87** 1365
[14] Gindhart A M, Lind C and Green M 2008 *J. Mater. Res.* **23** 210
[15] Marinkovic B A, Jardim P M, Ari M, de Avillez R R, Rizzo F and Ferreira F F 2008 *Phys. Status Solid B* **245** 2514
[16] Kimberly J M, Michel B J, Mary A W and Bojan A M 2012 *Solid State Commun.* **152** 1748
[17] Song W B, Liang E J, Liu X S, Li Z Y, Yuan B H and Wang J Q 2013 *Chin. Phys. Lett.* **30** 126502
[18] Liang E J, Huo H L, Wang J P and Chao M J 2008 *J. Phys. Chem. C* **112** 6577
[19] Ari M, Jardim P M, Marinkovic B A, Rizzo F and Ferreira F F 2008 *J. Solid State Chem.* **181** 1472
[20] Tyagi A K, Achary S N and Mathews M D 2002 *J. Alloys Compd.* **339** 207
[21] Mary T A and Sleight A W 1999 *J. Mater. Res.* **14** 912
[22] Kimberly J M, Carl P R, Mario B, Bojan A M, Luciana P and Mary A W 2013 *J. Am. Ceram. Soc.* **96** 561
[23] Suzuki T and Omote A 2006 *J. Am. Ceram. Soc.* **89** 691
[24] Li Z Y, Song W B and Liang E J 2011 *J. Phys. Chem. C* **115** 17806